# Quasi-Monte Carlo Estimation Approach for Denoising MRI Data Based on Regional Statistics

Alexander Wong*, *Member, IEEE*, and Akshaya K. Mishra, *Member, IEEE*

***Abstract*—An important postprocessing step for MR data is noise reduction. Noise in MR data is difficult to suppress due to its signal-dependence. To address this issue, a novel stochastic approach to noise reduction for MR data is presented. The estimation of the noise-free signal is formulated as a general Bayesian least-squares estimation problem and solved using a quasi-Monte Carlo method that takes into account the statistical characteristics of the underlying noise and the regional statistics of the observed signal in a data-adaptive manner. A set of experiments were performed to compare the proposed quasi-Monte Carlo estimation (QMCE) method to state-of-the-art wavelet-based MR noise reduction (WAVE) and nonlocal means MR noise reduction (NLM) methods using MR data volumes with synthetic noise, as well as real noise-contaminated MR data. Experimental results show that QMCE is capable of achieving state-of-the-art performance when compared to WAVE and NLM methods quantitatively in SNR, mean structural similarity (MSSIM), and contrast measures. Visual comparisons show that QMCE provides effective noise suppression, while better preserving tissue structural boundaries and restoring contrast.**

***Index Terms*—Bayesian, denoising, MR, noise reduction, quasi-Monte Carlo, regional statistics, stochastic.**

## I. Introduction

MRI is a medical imaging technique that has become a very powerful tool for clinical diagnosis as well as for studying the structural and functional characteristics of the body. MRI provides high contrast between tissues when compared to other imaging techniques without exposing patients to harmful ionizing radiation. While MRI technology has improved significantly over the years to provide improved resolution and SNR, as well as reduced acquisition times, there are still many fundamental tradeoffs between these three aspects due to operational, financial, and physical constraints. For example, it is necessary to constrain acquisition time from an operational perspective to alleviate patient discomfort and to improve the number of acquisitions that can be made within a certain period of time. However, constraining the acquisition time generally results in a decrease in SNR, which is undesirable. Therefore, low-level postprocessing methods for reducing noise in MRI are desired for both clinical visualization as well as higher level postprocessing operations, such as segmentation and tracking, whose performance can be greatly affected by the presence of noise.

Noise in MR data is a result of various factors, such as thermal noises from the patient and electronic noises from the MRI device [1], [2], and the noise-contaminated magnitude data is typically modeled as following a Rician distribution [3]. The main challenge in suppressing noise in MR data is that the noise statistics vary based on the underlying signal. Furthermore, a parametric model, such as the Rician distribution may not well model noise-contaminated data depending on the underlying MRI technology. Given the importance of noise reduction in MR data, various MR noise reduction techniques have been proposed in research literature over the years. One of the first MR noise reduction methods was proposed by McGibney and Smith [4], where the underlying signal is estimated as the linear weighted mean over a local neighborhood. Aja-Fernandez *et al.* [5] extended upon this approach by computing a linear minimum mean squared error estimate of the signal. Nonlinear approaches for estimating the signal were proposed by Gerig *et al.* [6] and Samsonov and Johnson [7], based on the concept of anisotropic diffusion proposed by Perona and Malik [8]. One issue with the aforementioned methods is that they rely solely on local neighborhood information, which may be insufficient for noise suppression under low SNR scenarios.

A popular class of approaches for MR noise reduction are wavelet-based methods [9]–[15]. In particular, Nowak [12] proposed incorporating the Rician distribution model into a threshold-based wavelet noise reduction framework, while Pirzurica *et al.* [13] introduced a wavelet noise reduction method based on estimates of the underlying noise distribution. One issue with wavelet-based methods is that they can introduce significant artifacts that relate to the wavelet being used. Another approach to MR noise reduction was taken by Sijbers *et al.* [16], [17], which estimates both the underlying signal and noise variance using a maximum-likelihood (ML) approach. More recently, Coupe *et al.* [18], Manjon *et al.* [19], and Wiest-Daesslé *et al.* [20] introduced MR noise suppression methods based on the nonlocal means method proposed by Buades *et al.* [21], [22], which was shown to provide good structural preservation even under low SNR scenarios, with [18] and [20] providing improved efficiency through a preselection process.

The main contribution of this paper is a novel stochastic noise reduction method for MR data. The proposed method utilizes a quasi-Monte Carlo estimation (QMCE) approach for estimating the noise-free signal, which learns the statistical characteristics of the underlying noise distribution, as well as taking into account the regional statistics of the observed signal, in a

Manuscript received September 11, 2009; revised October 30, 2009, January 28, 2010, and March 17, 2010; accepted March 18, 2010. Date of publication May 3, 2010; date of current version March 18, 2011. This work was supported by the Natural Sciences and Engineering Research Council of Canada. *Asterisk indicates corresponding author.*

*A. Wong is with the Department of Systems Design Engineering, University of Waterloo, Waterloo, ON N2L 3G1, Canada (e-mail: a28wong@uwaterloo.ca).

A. K. Mishra is with the Department of Systems Design Engineering, University of Waterloo, Waterloo, ON N2L 3G1, Canada (e-mail: akmishra@uwaterloo.ca).

Color versions of one or more of the figures in this paper are available online at http://ieeexplore.ieee.org.

Digital Object Identifier 10.1109/TBME.2010.2048325

data-adaptive manner. To the best of the authors' knowledge, there are no previous methods that have utilized such an approach to estimate the noise-free signal for MRI.

## II. Materials and Methods

### A. Problem Formulation

Let $X$ be a set of sites into a discrete lattice $\mathcal{S}$ upon which the MR data is defined and $x \in X$ be a site in $\mathcal{S}$. Let $M = \{M(x)|x \in X\}$, $A = \{A(x)|x \in X\}$, and $N = \{N(x)|x \in X\}$ be random fields on $X$, and $M(x)$, $A(x)$, and $N(x)$ be random variables representing the observed signal, the noise-free signal, and noise signal following a distribution $p$ at site $x$, respectively. Let $m = \{m(x)|x \in X\}$, $a = \{a(x)|x \in X\}$, and $n = \{n(x)|x \in X\}$ be realizations of $M$, $A$, and $N$, respectively. The problem of estimating the noise-free signal $a(x)$ from the observed signal $m(x)$ can be formulated as the following general Bayesian least-squares estimation problem:

$$\hat{a}(x) = \underset{\hat{a}(x)\in a(x)}{\arg\min}\{E[(a(x) - \hat{a}(x))^2|m(x)\forall x \in X]\}. \quad (1)$$

Minimizing the expression in (1) gives us the following expression:

$$\hat{a}(x) = \int p\left(a(x)|m(x)\right)a(x)da(x). \quad (2)$$

This means that the optimal estimate of the noise-free signal $a(x)$ is the mean conditioned on the observed signal $m(x)$. The problem of separating the noise-free signal $a(x)$ from the noise signal $n(x)$ is very challenging in two ways. First, no information is known about $a(x)$, making (2) impossible to solve directly. To work around this issue in a practical sense, a common approach used in numerical optimization is to use an initial estimate for $a(x)$, denoted as $a_0(x)$, in place of the actual $a(x)$. This gives us

$$\hat{a}(x) = \int p\left(a_0(x)|m(x)\right)a_0(x)da_0(x). \quad (3)$$

In the current implementation, the initial estimate of the noise-free signal ($a_0(x)$) is set to a smoothed version of $m(x)$ using a Gaussian kernel with unit standard deviation. Second, not only is the noise in MR data signal-dependent, the noise distribution can vary depending on the underlying MRI technique. Therefore, solving for $a(x)$ based on (2) can be very challenging given the highly complex nature of the posterior distribution $p\left(a_0(x)|m(x)\right)$. A common approach to addressing this issue is to instead utilize a linear least-squares approximation of the problem, based on parametric distribution models, such as the Rician distribution [5]. However, such approximations can be a poor fit given the highly complex nature of MR imagery, thus resulting in poor signal estimates. Even nonlinear approximations of the problem based on single-point statistics can lead to poor signal estimates given the physical relationships between tissues that are captured in MR data. To account for such physical relationships between tissues and the statistical characteristics of the MR data in a data-adaptive manner, we propose to instead employ a quasi-Monte Carlo approach to estimating $a(x)$ based on regional statistics.

### B. Quasi-Monte Carlo Method Based on Regional Statistics

The primary challenge to estimating $a(x)$ using (2) is in obtaining a reliable estimate of $p\left(a_0(x)|m(x)\right)$. Rather than utilizing a parametric distribution model or nonparametric distribution models based on single-point statistics, which can be a poor fit for the underlying MR data due to factors, such as imaging technique and physical tissue relationships, we instead estimate $p\left(a_0(x)|m(x)\right)$ using the following quasi-Monte Carlo approach based on regional statistics.

First, a set of $n$ samples $\{x_{j=1,\ldots,n}\}$ is drawn from $a_0(x)$ using a Sobol quasi-random sequence $Q(x)$ to promote low sample discrepancies [23]. To account for physical tissue relationships captured in MR data, we wish to utilize regional statistics rather than single-point statistics. Let us define a local region around a site $x$, denoted as $\rho(x)$, as all samples $x_i$ in the image such that $\|x - x_i\|_2 \leq r$, where $r$ defines the radius of the local region. Therefore, to determine the inclusion of $x_j$ as a sample used to estimate $p\left(a_0(x)|m(x)\right)$, we first measure the degree of likelihood $\mathcal{L}$ of the local region around $x_j$, denoted as $\rho(x_j)$, belonging to the same distribution as the local region of the site being estimated, denoted as $\rho(x)$, which we model based on the error $\varepsilon = m_{\rho(x)} - a_{0\,\rho(x_j)}$ between the local regions

$$\mathcal{L}(\rho(x_j), \rho(x)) = \prod_{i=1}^{n_\rho} f(\varepsilon(i)|\rho(x_j), \rho(x)) \quad (4)$$

where $i$ is the $i$th sample in the local region, $n_\rho$ is the number of samples in a local region, and $f(\varepsilon(i)|\rho(x_j), \rho(x))$ is a conditional functional with respect to the regions. The motivation behind the inclusion of samples for estimating $p\left(a_0(x)|m(x)\right)$ based on the degree of likelihood $\mathcal{L}$ is that samples with similar physical tissue relationships as that of $x$ provide more relevant information with regards to $a(x)$ than those with dissimilar physical tissue relationships.

To integrate noise statistics in $\mathcal{L}$, we propose the following noise-adaptive Gibbs-based energy functional, designed such that the energy functional approaches zero within two noise standard deviations

$$f(\varepsilon(i)|\rho(x_j), \rho(x)) = \exp\left[-\frac{4\left(m_{\rho(x)}(i) - a_{0\,\rho(x_j)}(i)\right)^2}{Z\sigma^2}\right] \quad (5)$$

where $m_{\rho(x)}(i)$ and $a_{0\,\rho(x_j)}(i)$ are the observed signal and the initial estimate of the $i$th sample in regions $\rho(x)$ and $\rho(x_j)$, respectively, $Z$ is the number of sites in a region, and $\sigma$ is the noise standard deviation and can be estimated as the square root of the expected value of the squared background intensities [19]. By designing $\mathcal{L}$ based on a likelihood cutoff of approximately two noise standard deviations, we have accounted for the underlying noise in the image. The use of two noise standard deviations is motivated by parametric tests presented in Section III.

To further reduce the influence of outlier noise on the estimation of $a(x)$, particularly in low SNR scenarios, where $\mathcal{L}$ is relatively low across all samples, we wish to only include samples satisfying the following likelihood criterion based on the degree of regional likelihood $\mathcal{L}$ for inclusion in estimating

$p\left(a_0(x)|m(x)\right)$:

$$\mathcal{L}(\rho(x_j),\rho(x)) > \tau \tag{6}$$

where $\tau$ is the acceptance threshold. We can derive the acceptance threshold $\tau$ by enforcing the same "two noise standard deviations" criterion used in the design of (5) into (6). Replacing the $\left(m_{\rho(x)}(x_i) - a_{0\,\rho(x_j)}(x_i)\right)$ term with $2\sigma$ in (5) and substituting it into (6) gives

$$\mathcal{L}(\rho(x_j),\rho(x)) > \prod_{i=1}^{n_\rho} \exp\left[-\frac{4\left(2\sigma\right)^2}{Z\sigma^2}\right]. \tag{7}$$

Therefore, the acceptance threshold $\tau$ becomes

$$\tau = \prod_{i=1}^{n_\rho} \exp\left[-\frac{16}{Z}\right]. \tag{8}$$

Given the remaining samples satisfying (6), let $\Omega$ be the set of $v$ samples $\{x_{k=1,\ldots,v}\}$ selected for the estimation of $p\left(a_0(x)|m(x)\right)$. Given $\Omega$, the Monte Carlo posterior distribution estimate $\hat{p}\left(a_0(x)|m(x)\right)$ can be determined as follows:

$$\hat{p}\left(a_0(x)|m(x)\right) = \frac{p^*\left(a_0(x)|m(x)\right)}{\int p^*\left(a_0(x)|m(x)\right) da_0(x)} \tag{9}$$

$$p^*\left(a_0(x)|m(x)\right) = \frac{1}{\sqrt{2\pi}\sigma} \sum_{k=\Omega} \mathcal{L}(\rho(x_k),\rho(x)) \times \exp\left(-\frac{1}{2}\left(\frac{a_0 - m(x_k)}{\sigma}\right)^2\right). \tag{10}$$

Integrating the regional likelihood $\mathcal{L}$ as an objective function for the Monte Carlo posterior distribution estimate in (9) allows for samples with high regional likelihood to have greater influence on the estimation of $p\left(a_0(x)|m(x)\right)$ and improves the quality of the estimate of the noise-free signal.

Given (9), the noise-free signal $a(x)$ can be estimated as follows:

$$\hat{a}(x) = \int \hat{p}\left(a_0(x)|m(x)\right) a_0(x) da_0(x). \tag{11}$$

### C. Handling MR Magnitude Data

There are situations, where noise reduction must be performed on MR magnitude data. As discussed in [12], there exists a noise bias of $2\sigma^2$ in the squared magnitude of the MR signal that can be removed by simply subtracting the bias to recover the noise-free signal. Therefore, an unbiased estimate of the magnitude of the noise-free signal, denoted as $|\hat{a}|$, based on the proposed QMCE approach can be defined as follows [19], [20]:

$$|\hat{a}(x)| = \sqrt{\left(\int \hat{p}\left(a_0(x)|m(x)\right) a_0^2(x) da_0(x)\right) - 2\sigma^2}. \tag{12}$$

Based on the formulation in (12), it is possible that the term under the square root is negative. For these cases, $|\hat{a}|$ is set to zero. As pointed out by Wiest-Daesslé *et al.* [20], negative values are mainly found in the background of the images in real data.

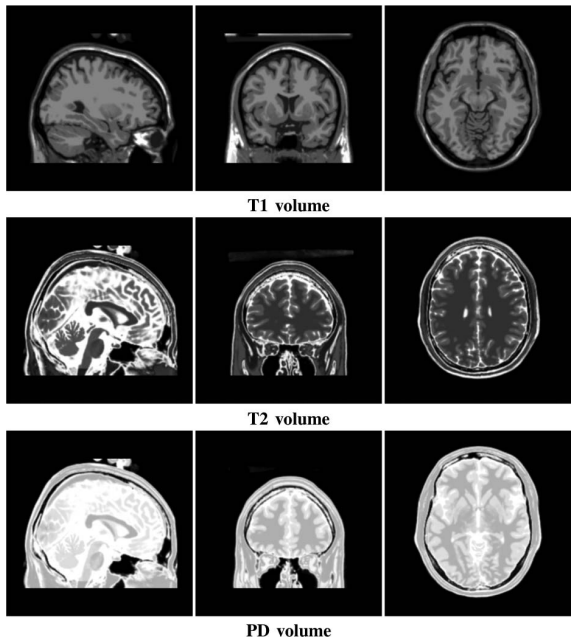


Fig. 1. Noise-free MR volumes used in experiment from the BrainWeb phantom [24].

## III. Experimental Results

To evaluate the effectiveness of QMCE for denoising MRI data, three sets of experiments involving both synthetic 3-D MR data with simulated Rician noise and real noise-contaminated 3-D MR data were performed. For comparison purposes, the state-of-the-art wavelet-based MR noise reduction method (WAVE) proposed by Pizurica *et al.* [13] and the state-of-the-art nonlocal means MR noise reduction method (NLM) proposed in Wiest-Daesslé *et al.* [20] were also evaluated. Note that NLM and QMCE are implemented such that the noise reduction is performed in 3-D, whereas WAVE performed noise reduction in 2-D for individual slices. All tested methods were implemented using the parameters proposed in the associated research literature, with a $11 \times 11 \times 11$ search volume, a $5 \times 5 \times 5$ local neighborhood, and $h = \sigma$ used for NLM based on [20]. For testing purposes, $n$ was set to 200 as it was shown through experimentation across the range $50 \leq n \leq 500$ that little improvement in average SNR is observed across all tested data beyond $n = 200$. Also, it was shown by Wiest-Daesslé *et al.* [20] that setting the radius of the local region $r$ to 2 provides the optimal average SNR based on empirical testing, and therefore, this setting was used during testing. QMCE was implemented in MATLAB and tested on an Intel Pentium 4 3 GHz machine with 1 GB of RAM.

### A. Experiment 1: SNR and Mean Structural Similarity Evaluation

In the first set of experiments, we investigate the effectiveness of QMCE for suppressing different levels of Rician noise. This gives us a good sense empirically on how much noise is reduced by QMCE. To achieve this goal, three noise-free simulated MR volumes (PD, *T*1, and *T*2), with voxel resolution of 1 $\text{mm}^3$ and 8-bit quantization, from the BrainWeb phantom [24]

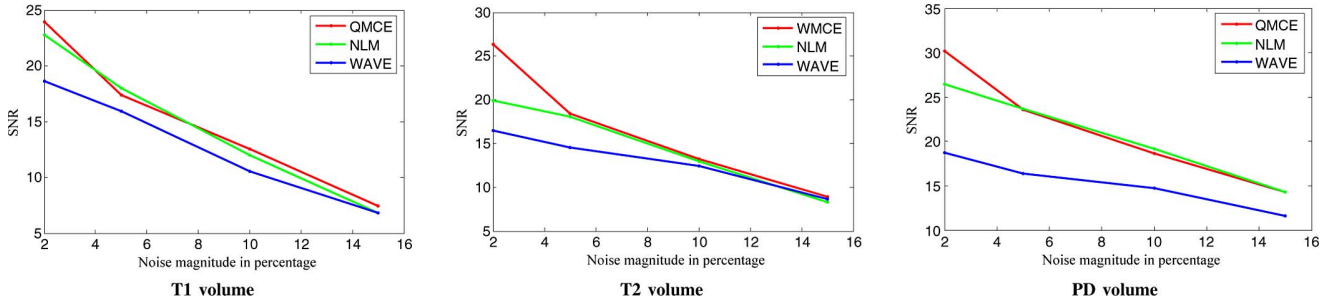


Fig. 2. SNRs of the estimates of the noise-free signals with respect to Rician noise standard deviation $\sigma$. QMCE produced estimates with noticeably higher SNRs than WAVE for all tested noise levels, while achieving comparable SNRs when compared to NLM.

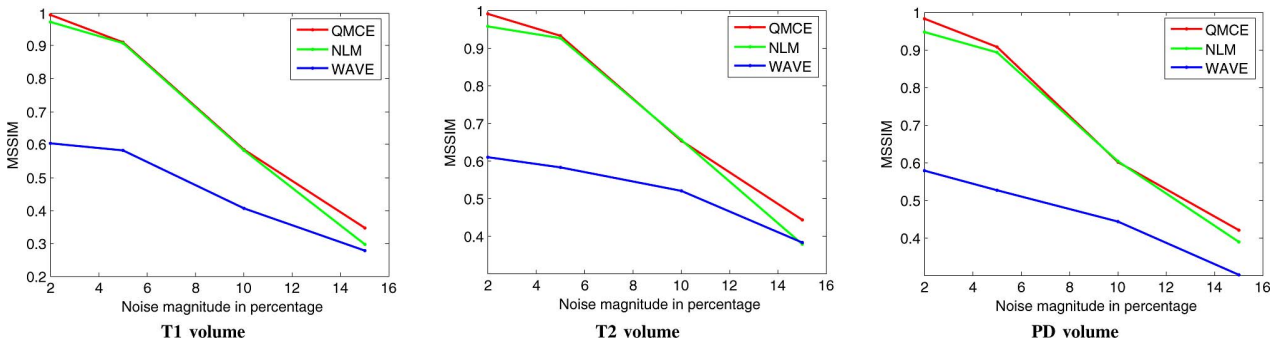


Fig. 3. MSSIM measures [25] of the estimates of the noise-free signals with respect to Rician noise standard deviation $\sigma$. QMCE produced estimates with noticeably higher MSSIM values than WAVE for all tested noise levels, while achieving comparable MSSIM values when compared to NLM.

was contaminated by simulated Rician noise with standard deviations $\sigma = \{2\%, 5\%, 10\%, 15\%\}$ of the dynamic range. The noise-free MR volumes used as the basis for this set of experiments are shown in Fig. 1. To contaminate the MR volumes with simulated Rician noise, the real and imaginary parts of the simulated MR volumes was contaminated with zero-mean Gaussian noise [19]. For visualization purposes, the magnitude of the MR volumes is shown. The noise-contaminated MR volumes are then processed using the tested methods and the SNR, as described in [13], and the mean structural similarity (MSSIM) value [25] was measured. The SNR measure was computed according to the following formula [13]:

$$\mathrm{SNR}\,(\hat{a}) = 10\log_{10}\left(\frac{\mathrm{Var}(a)}{\mathrm{Var}(\hat{a}-a)}\right) \tag{13}$$

where $\mathrm{Var}(a)$ is the variance of the noise-free reference data and $\mathrm{Var}(\hat{a}-a)$ is the noise variance. The SNR measure provides an indication of how accurate the reconstructed signal is compared to the original noise-free signal, where a high SNR value indicates strong signal fidelity and accurate signal reconstruction. The MSSIM measure provides a good indication of how well image details are preserved in the reconstructed signal compared to the original noise-free signal. High MSSIM values indicate strong detail preservation in the reconstructed signal, which is very important for clinical visualization and diagnosis of disease.

Plots of the SNRs and MSSIM values of the estimates of the noise-free signals with respect to Rician noise standard deviation $\sigma$ are shown in Figs. 2 and 3, respectively. QMCE produced estimates with noticeably higher SNRs and MSSIM values than WAVE for all tested Rician noise standard deviations, while achieving comparable SNRs and MSSIM values when compared to NLM. An example slice of the signal estimate for the *T*2 volume at the tested Rician noise standard deviations is shown in Fig. 4. The signal estimate produced by WAVE contains significant artifacts that relate to the underlying wavelet used. These artifacts are particularly noticeable in the homogeneous regions of the white matter, where band-like structures are formed that do not appear in the original noise-free data. The estimates produced by NLM and QMCE do not contain such artifacts and better preserve structural characteristics as well as suppress noise at all noise levels, with QMCE providing an improvement in sharpness of structural characteristics at high noise levels. A closeup of an example slice of the signal estimate for the *T*1 volume at 5% simulated Rician noise is shown in Fig. 5. On close visual inspection, NLM and QMCE performed noticeably better at estimating the noise-free signal than WAVE, which is contaminated by significant artifacts. As with the previous example, QMCE provides improvement in sharpness of structural characteristics when compared to NLM, particularly in the gray matter regions.

### *B. Experiment 2: Contrast Evaluation*

In the second set of experiments, we investigate the effectiveness of QMCE at restoring the contrast in MR data under different levels of simulated Rician noise. This gives us a good

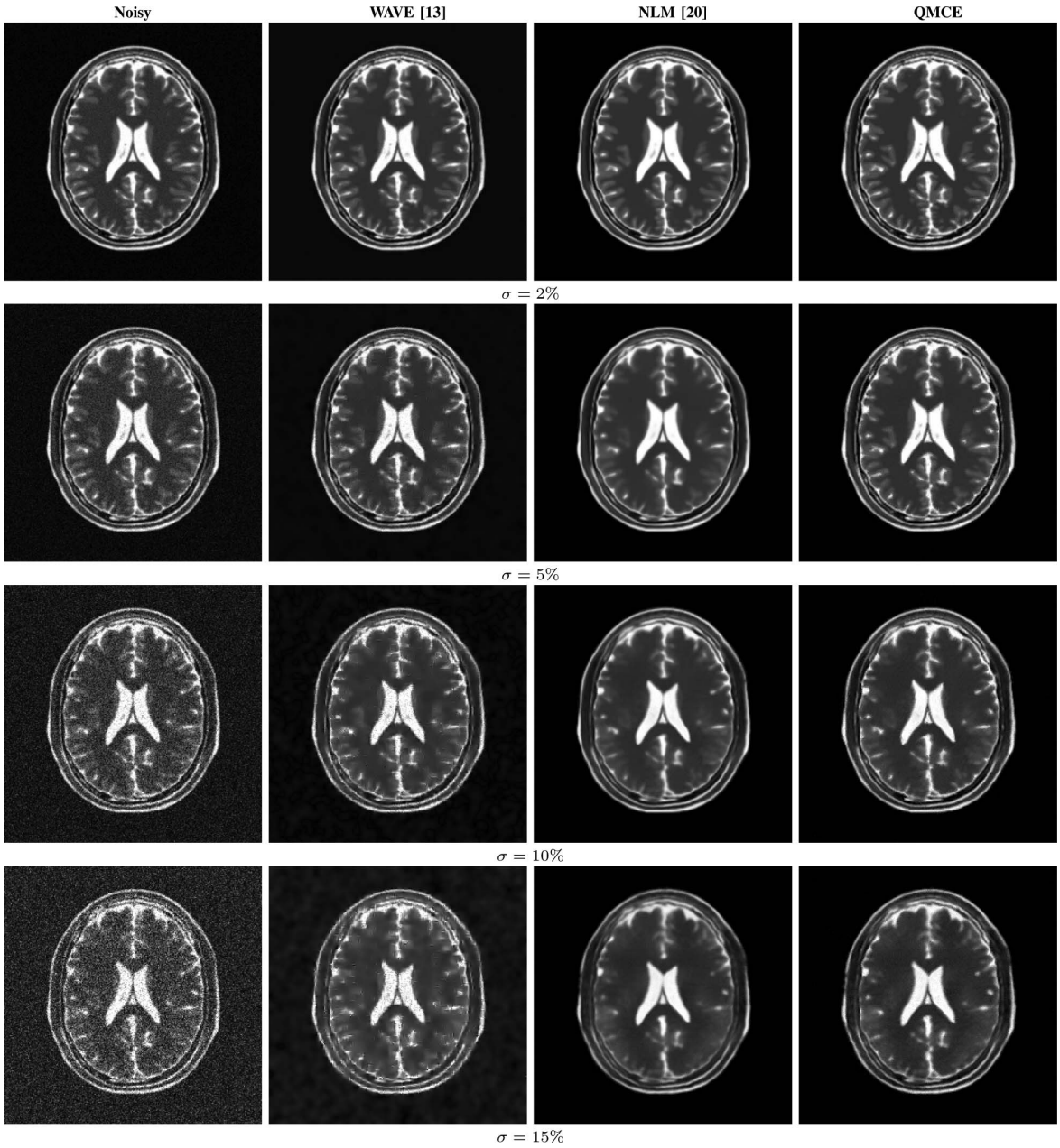


Fig. 4. Example of slice of the estimate of the noise-free signal produced by the WAVE [13], NLM [20], and QMCE methods for the *T*2 volume at different Rician noise standard deviations. The signal estimate produced by WAVE contains significant artifacts that relate to the underlying wavelet used. The estimates of the noise-free signals produced by NLM and QMCE do not contain such artifacts and better preserve structural characteristics as well as suppress noise at all noise levels, with QMCE providing an improvement in sharpness of structural characteristics at high noise levels, particularly in the gray matter regions.

sense empirically on how well different features such as tissues can be distinguished in the estimated noise-free signal, which is important for visual interpretation and analysis. To achieve this goal, the noise-free volumes used in the first set of experiments was contaminated by simulated Rician noise with standard deviations $\sigma = \{2\%, 5\%, 10\%, 15\%\}$ of the dynamic range. The noise-contaminated MR volumes are then processed using the tested methods and the contrast $c$ was measured as follows [12]:

$$c = \left(\frac{E(a_1) + E(a_2)}{E(a_1) - E(a_2)}\right)\left(\frac{E(\hat{a}_1) - E(\hat{a}_2)}{E(\hat{a}_1) + E(\hat{a}_2)}\right) \qquad (14)$$

where $E(a_1)$ and $E(a_2)$ are the expected values of the dark regions and bright regions of $a$, respectively, and $E(\hat{a}_1)$ and $E(\hat{a}_2)$ are the expected values of the dark regions and bright regions of $\hat{a}$, respectively.

Plots of the contrast of the signal estimates with respect to Rician noise standard deviation $\sigma$ are shown in Fig. 6. QMCE produced signal estimates with comparable contrast as NLM for all tested Rician noise standard deviations, with WAVE performing noticeably worst. Furthermore, the ability of the WAVE to restore contrast decreases significant as $\sigma$ increases. Both NLM and QMCE are able to restore noticeably more contrast in the estimated signal at all values of $\sigma$ when compared to WAVE.

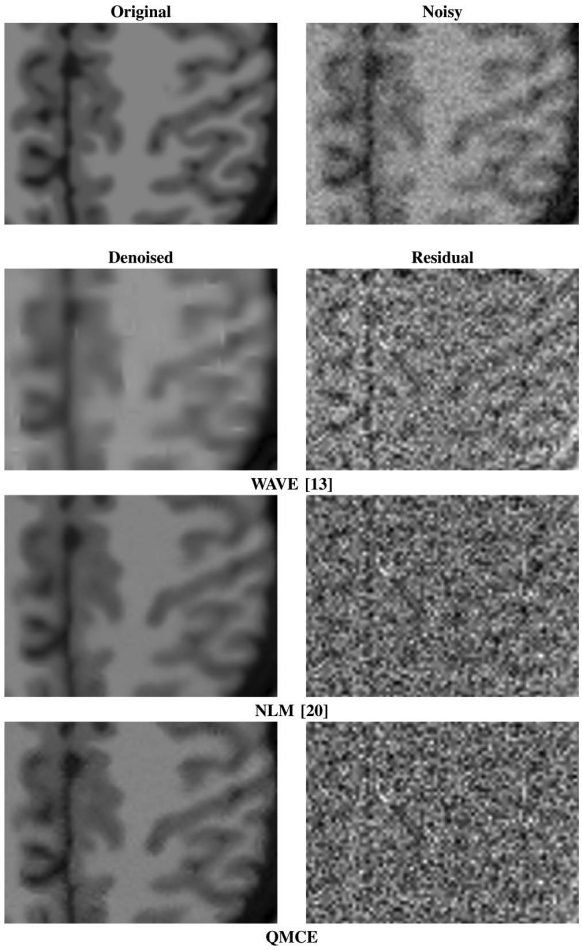


Fig. 5. Closeup of an example slice of the signal estimate of the noise-free signal for the *T*1 volume at 5% simulated Rician noise produced by the WAVE [13], NLM [20], and QMCE methods, and their corresponding residuals. There is noticeable artifacts in the estimate produced by WAVE in the homogeneous regions of the white matter, where band-like structures are formed that do not appear in the original noise-free data and curved structures formed by gray matter have a blocky appearance.

### C. Experiment 3: Real-Noisy MR Data

In the third set of experiments, we investigate the effectiveness of QMCE at reducing noise in real noise-contaminated MR data. This gives us a good sense subjectively on how well QMCE performs in real-world situations, and thus, validate its operation applicability. To achieve this goal, a real patient MR/*T*1 brain volume, with a slice thickness of 5-mm and 8-bit quantization, of a 76-year-old male with chronic subdural hematoma [26] was processed using the tested methods. Given that this is real noise-contaminated MR data, the noise-free data is unavailable and as such the effectiveness of denoising will be evaluated visually. The noise $\sigma$ was estimated as the square root of the expected value of the squared background intensities [19], although other approaches such as that produced by Aja-Fernandez *et al.* [27] may provide more robust estimates in the situation, where ghosting artifacts exist in the data. The magnitude of three slices from the signal estimate of the real noise-contaminated MR data are shown in Fig. 7. As with the first set of experiments, NLM and QMCE is able to better preserve structural characteristics, while suppressing the underlying noise when compared to WAVE. Furthermore, the signal estimate produced by both NLM and QMCE does not exhibit the significant artifacts contained in that proposed by WAVE, which is most noticeable in the homogeneous regions of the white matter, where band-like structures are formed that do not appear in the original noise-free data. The signal estimates produced by QMCE exhibit sharper structural characteristics than NLM, particularly in the gray matter regions.

### D. Experiment 4: Choice of Acceptance Criterion

In Section II-B, we utilized a "two standard deviations" acceptance criterion to derive the acceptance threshold $\tau$. To justify the choice of this acceptance criterion, we investigate the effectiveness of QMCE at reducing noise for suppressing different levels of Rician noise given different acceptance criteria. This gives us a good sense empirically on what is a suitable acceptance criterion for deriving $\tau$. To achieve this goal, the three noise-free simulated MR volumes (PD, *T*1, and *T*2) used in Section III-A are contaminated by simulated Rician noise with standard deviations $\sigma = \{5\%, 15\%\}$ of the dynamic range. The noise-contaminated MR volumes are then processed using QMCE for different acceptance criteria from $0.1\tau$ to $11\tau$ and the average SNR was measured.

Plots of the average SNRs with respect to acceptance criterion for Rician noise standard deviation $\sigma = \{5\%, 15\%\}$ are shown in Fig. 8. QMCE produced the highest average SNRs for both $\sigma = 5\%$ and $\sigma = 15\%$ when the acceptance criterion is set up $2\sigma$, thus empirically providing justification for the use of the "two standard deviations" acceptance criterion used to derive $\tau$.

## IV. Computational Cost Analysis

In the third set of experiments, we investigate the computational cost of performing QMCE relative to the other tested methods. To achieve this goal, the execution time of all three tested methods was recorded for denoising the three simulated MR volumes from the BrainWeb phantom [24] used in the first set experiments. Each volume consists of $181 \times 217 \times 181$ voxels, with a voxel resolution of 1 mm$^3$. At 1.09 s per slice, WAVE performs significantly faster than either NLM or QMCE, although the level of denoising performance is significantly worse than the other two methods, as shown in previous experiments. Despite being slower than WAVE, the execution time of QMCE at 15.67 s per slice is noticeably faster than that of NLM at 96.95 s per slice, while achieving similarly high levels of noise reduction and structure preservation. This difference in execution time between NLM and QMCE can be attributed to the fact that NLM uses a large number of pixels, many of which have low relevancy to estimate the noise-free signal, whereas QMCE uses a small set of samples with high relevancy, and thus, require significantly fewer computations. Given the independent nature of performing QMCE on each voxel, one effective approach to significantly reducing execution time is by employing a parallel processing framework, where multiple voxels are processed using QMCE in parallel.

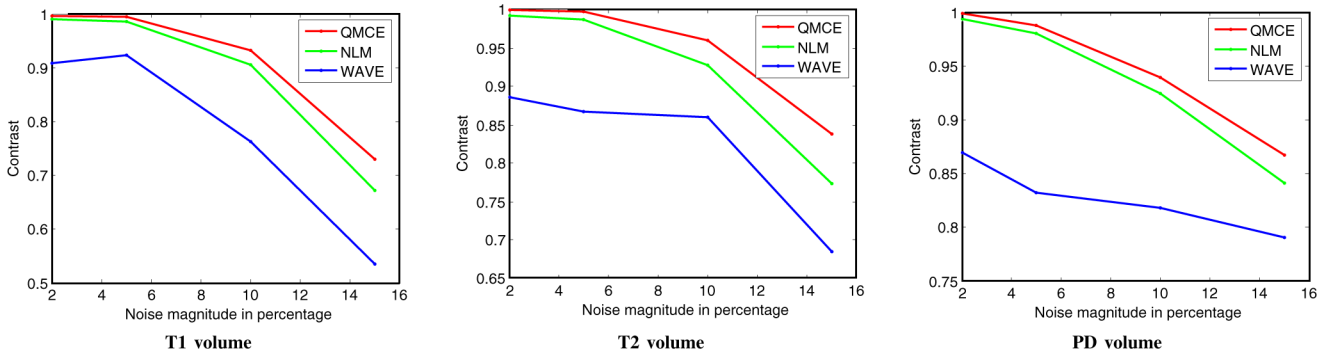


Fig. 6. Contrast of the signal estimates with respect to Rician noise standard deviation $\sigma$.

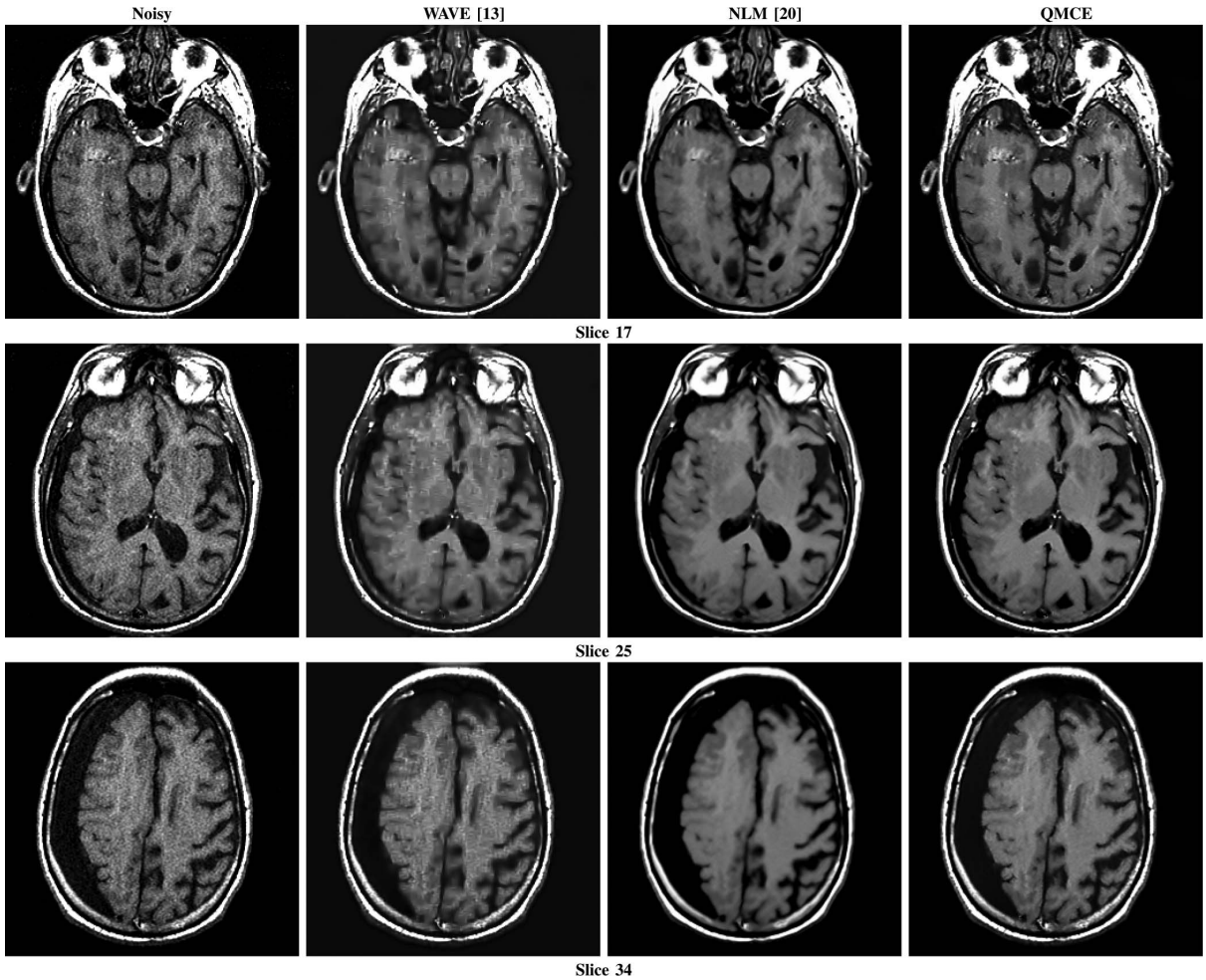


Fig. 7. Example slices from the signal estimates produced by WAVE [13], NLM [20], and QMCE for real noise-contaminated MR data. As with the first set of experiments, NLM and QMCE is able to better preserve structural characteristics, while suppressing the underlying noise when compared to WAVE. Furthermore, the signal estimate produced by both NLM and QMCE does not exhibit the significant artifacts contained in that proposed by WAVE, which is most noticeable in the homogeneous regions of the white matter, where band-like structures are formed that do not appear in the original noise-free data. The signal estimates produced by QMCE exhibit sharper structural characteristics than NLM, particularly in the gray matter regions.

## V. Conclusion

In this paper, a novel stochastic approach for denoising MR data was introduced. A general Bayesian least-squares formulation of the noise-free signal estimation problem was presented and a QMCE approach was introduced for solving the problem in a reliable manner based on regional statistics. Experimental results show that QMCE provides state-of-the-art performance compared to both the WAVE and NLM methods quantitatively in SNR, MSSIM, and contrast measures. Furthermore, visual comparisons show that QMCE provides noticeably improved tissue structural preservation and higher contrast without significant artifacts. Future work involves investigating the operational

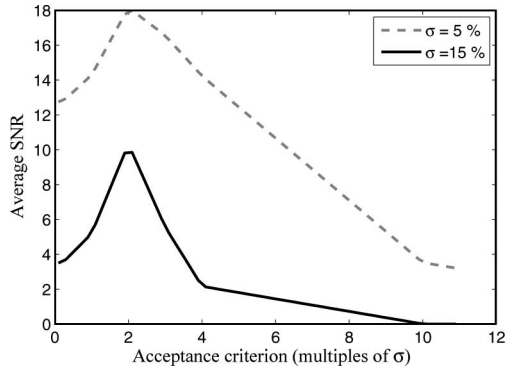


Fig. 8. Average SNRs with respect to acceptance criterion for Rician noise standard deviation $\sigma = \{5\%, 15\%\}$ QMCE produced the highest average SNRs for both cases when the acceptance criterion is set to $2\sigma$.

application of QMCE on various MRI and spectroscopy applications, such as functional MRI and diffusion-weighted MRI.

## ACKNOWLEDGMENT

The authors would like to thank Dr. K. A. Johnson from the Harvard Medical School for the test data.

## REFERENCES

[1] W. Edelstein, G. Glover, C. Hardy, and R. Redington, "The intrinsic signal-to-noise ratio in NMR imaging," *Magn. Reson. Med.*, vol. 3, pp. 604–618, 1986.

[2] E. McVeigh, R. Henkelman, and M. Bronskill, "Noise and filtration in magnetic resonance imaging," *Med. Phys.*, vol. 12, pp. 586–591, 1985.

[3] S. Rice, "Statistical properties of a sine-wave plus random noise," *Bell Syst. Tech. J.*, vol. 27, pp. 109–157, 1948.

[4] G. McGibney and M. Smith, "Unbiased signal-to-noise ratio measure for magnetic resonance images," *Med. Phys.*, vol. 20, no. 4, pp. 1077–1078, 1993.

[5] S. Aja-Fernandez, M. Niethammer, M. Kubicki, M. Shenton, and C. Westin, "Restoration of DWI data using a rician LMMSE estimator," *IEEE Trans. Med. Imag.*, vol. 27, no. 10, pp. 1389–1403, Oct. 2008.

[6] G. Gerig, O. Kubler, R. Kikinis, and F. Jolesz, "Nonlinear anisotropic filtering of MRI data," *IEEE Trans. Med. Imag.*, vol. 11, no. 2, pp. 221–232, Jun. 1992.

[7] A. Samsonov and C. Johnson, "Noise-adaptive nonlinear diffusion filtering of MR images with spatially varying noise levels," *Magn. Reson. Med.*, vol. 52, pp. 798–806, 2004.

[8] P. Perona and J. Malik, "Scale-space and edge detection using anisotropic diffusion," *IEEE Trans. Pattern Anal. Mach. Intell.*, vol. 12, no. 7, pp. 629–639, Jul. 1990.

[9] J. Weaver, Y. Xu, D. Healy, and J. Driscoll, "Filtering MR images in the wavelet transform domain," *Magn. Reson. Med.*, vol. 21, pp. 288–295, 1991.

[10] Y. Xu, J. Weaver, D. Healy, and J. Lu, "Wavelet transform domain filters: A spatially selective noise filtration technique," *IEEE Trans. Image Process.*, vol. 3, no. 6, pp. 747–758, Nov. 1994.

[11] M. Hilton, T. Ogden, D. Hattery, G. Jawerth, and B. Eden, "Wavelet denoising of functional MRI data," in *Wavelets in Medicine and Biology*. Boca Raton, FL: CRC Press, 1996.

[12] R. Nowak, "Wavelet-based Rician noise removal for magnetic resonance imaging," *IEEE Trans. Image Process.*, vol. 8, no. 10, pp. 1408–1419, Oct. 1999.

[13] A. Pizurica, W. Philips, I. Lemahieu, and M. Acheroy, "A versatile wavelet domain noise filtration technique for medical imaging," *IEEE Trans. Med. Imag.*, vol. 22, no. 3, pp. 323–331, Mar. 2003.

[14] A. Wink and J. Roerdink, "Denoising functional MR images: A comparison of wavelet denoising and Gaussian smoothing," *IEEE Trans. Med. Imag.*, vol. 23, no. 3, pp. 374–387, Mar. 2004.

[15] A. Pizurica, A. Wink, E. Vansteenkiste, W. Philips, and J. Roerdink, "A review of wavelet denoising in MRI and ultrasound brain imaging," *Curr. Med. Imag. Rev.*, vol. 2, no. 2, pp. 247–260, 2006.

[16] J. Sijbers, A. den Dekker, P. Scheunders, and D. Van Dyck, "Maximum-likelihood estimation of Rician distribution parameters," *IEEE Trans. Med. Imag.*, vol. 17, no. 3, pp. 357–361, Jun. 1998.

[17] J. Sijbers and A. den Dekker, "Maximum likelihood estimation of signal amplitude and noise variance form MR data," *Magn. Reson. Imag.*, vol. 51, pp. 586–594, 2004.

[18] P. Coupé, P. Yger, S. Prima, P. Hellier, C. Kervrann, and C. Barillot, "An optimized blockwise nonlocal means denoising filter for 3-D magnetic resonance images," *IEEE Trans. Med. Imag.*, vol. 27, no. 4, pp. 425–441, Apr. 2008.

[19] J. Manjon, J. Carbonell-Caballero, J. Lull, G. Garcia-Marti, L. Marty-Bonmaty, and M. Robles, "MRI denoising using non-local means," *Med. Image Anal.*, vol. 12, pp. 514–523, 2008.

[20] N. Wiest-Daesslé, S. Prima, P. Coupé, S. Morrissey, and C. Barillot, "Rician noise removal by non-local means filtering for low signal-to-noise ratio MRI: Applications to DT-MRI," *Med. Image Comput. Comput. Assist. Interv.*, vol. 11, no. 2, pp. 171–179, 2008.

[21] A. Buades, B. Coll, and J. Morel, "A review of image denoising algorithms, with a new one," *Multiscale Model. Simul.*, vol. 4, no. 2, pp. 490–530, 2005.

[22] A. Buades, B. Coll, and J. Morel, "Nonlocal image and movie denoising," *Int. J. Comput. Vis.*, vol. 76, no. 2, pp. 123–140, 2008.

[23] I. Sobol, "Uniformly distributed sequences with an additional uniform property," *USSR Comput. Math. Math. Phys.*, vol. 16, pp. 236–242, 1997.

[24] C. Cocosco, V. Kollokian, R. Kwan, and A. Evans, "BrainWeb: Online interface to a 3D MRI simulated brain database," *NeuroImage*, vol. 5, no. 4, p. S425, 1997.

[25] Z. Wang, A. Bovik, H. Sheikh, and E. Simoncelli, "Image quality assessment: From error measurement to structural similarity," *IEEE Trans. Image Process.*, vol. 13, no. 4, pp. 600–612, Apr. 2004.

[26] K. Johnson and J. Becker, The whole brain atlas. (2010). [Online]. Available: http://www. med.harvard.edu/AANLIB/home.html

[27] S. Aja-Fernandez, M. Martin-Fernandez, and C. Alberola-Lopez, "Automatic noise estimation in images using local statistics. Additive and multiplicative cases," *Image Vis. Comput.*, vol. 27, no. 6, pp. 756–770, 2009.

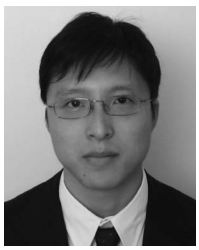

**Alexander Wong** (M'05) received the B.Sc. degree in computer engineering, the M.Sc. degree in electrical and computer engineering, and the Ph.D. degree in systems design engineering in 2005, 2007, and 2010, respectively, from the University of Waterloo, Waterloo, ON, Canada.

He is also with the Vision and Image Processing Research Group, University of Waterloo. He has authored or coauthored papers in various fields such as computer vision, graphics, image processing, biomedical signal processing, and multimedia systems, published in refereed journals and conferences. His current research interests include biomedical image processing and analysis, computer vision, and pattern recognition. He is involved in various projects on image registration, image denoising, image superresolution, image segmentation, biomedical tracking, biomedical image analysis, and image and video coding.

**Akshaya K. Mishra** (M'07) received the M.Tech degree from the Indian Institute of Technology (IIT), Kharagpur, India, in 2004. Currently, he is working toward the Ph.D. degree at the University of Waterloo.

He worked as a Research Engineer at Read-Ink Technology Pvt Ltd., Bangalore, India from 2004 to 2006, where he was working on developing architecture for on-line and off-line handwritten character recognition. He has published several refereed journal and conference papers in diverse fields of biomedical image processing, pattern recognition, denoising and computer vision. His research interest includes medical image analysis, handwritten character recognition, active contour based image and video segmentation, tracking, denoising and data fusion.